Supporting Information

Sacino et al. 10.1073/pnas.1321785111

SI Materials and Methods

Expression and Purification of Recombinant αS Proteins. Recombinant N-terminal truncated 21–140 human α-synuclein (αS) (with a Met codon added before amino acid 21), 71–82 deletion (Δ71–82) human αS, and full-length mouse αS were expressed and purified to homogeneity as previously described (1–3). The 21–140 human αS was shown to induce αS inclusion formation similar to full-length protein in cultured cells (4, 5) but provided the added advantage of being able to determine that inclusions are comprised of the endogenously expressed αS using N-terminal αS antibodies (6, 7). The Δ71–82 αS has a deletion in the middle of the hydrophobic region of αS that is required for amyloid formation and therefore lacks the ability to form or seed αS amyloid in vitro and in vivo under physiological conditions (1, 2, 4, 8).

Fibril Preparation of Recombinant αS for Injection. αS protein was assembled into filaments by incubation at 37 °C at 5 mg/mL in sterile PBS (Invitrogen) with continuous shaking at 1,050 rpm (Thermomixer R; Eppendorf) for 48 h. αS amyloid fibril assembly was monitored as previously described with K114 fluorometry (2, 9). αS fibrils were diluted in sterile PBS and treated by mild water bath sonication for 2 h at room temperature. These fibrils were tested for induction of intracellular amyloid inclusion formation as previously described (5). The Δ71–82 αS used for the current studies was not preincubated and is in the soluble form as previously described (1, 2). We have also recently shown that this same preparation of Δ71–82 αS cannot directly seed the formation of αS inclusions in primary neuronal culture. In contrast, the same preparation of fibrillar αS can seed inclusion formation very efficiently in those cultures (8).

Immunohistochemical Analysis. Mice were killed with CO_2 euthanization and perfused with PBS/heparin. The brain and spinal cord were then removed and fixed for at least 48 h in 70% ethanol/150 mM NaCl or neutral buffered formalin followed by paraffin infiltration. Paraffin-embedded tissue blocks were cut in 7-μm sections that were immunostained using previously described methods and immunocomplex visualization via chromogen 3,3′-diaminobenzidine (10). Sections also were counterstained with hematoxylin. All slides were scanned using an Aperio ScanScope CS (40× magnification; Aperio Technologies), and images of representative areas were taken using the ImageScope software (40× magnification; Aperio Technologies). Quantification of immunoreactivity for the levels of astrogliosis and microgliosis was accomplished using ImageScope software to measure the density of staining per area. Three independent regions were quantified per animal, and two animals were used per condition. The data are expressed as averaged immunoreactivity per area normalized to the control ± SEM. Stained tissue sections from untreated young (3 mo to 4 mo) M83 transgenic (Tg) mice without αS inclusion pathology were used as the baseline control.

Muscle Histology. Whole-mount flexor digitorum brevis muscles were placed into ice-cold PBS for less than 10 min to remove connective tissue and gently spread the muscle bundles using sharp forceps. Tissues were fixed with 4% paraformaldehyde in PBS for 20 min at room temperature, rinsed, and processed for immunostaining as described (11). Whole mounts were incubated in blocking buffer (PBS with 1% Triton X-100, 5% normal goat serum, and 1% BSA) overnight at 4 °C and then incubated in chicken anti-neurofilament-H (1:3,000; Encore Biotechnology) and mouse monoclonal anti-syntaptotagmin (1:1,000; Developmental Studies Hybridoma Bank) antibodies in diluting buffer for 24 h at 4 °C. Whole mounts were washed in PBS for 3 h, followed by incubation in Alexa-488 goat anti-chicken and Alexa-488 goat anti-mouse secondary antibodies and Alexa-594 α-bungarotoxin (all from Invitrogen) overnight at 4 °C. After washing for 3 h in PBS, samples were mounted on slides in ProLong Antifade mounting media (Invitrogen). Quantification of the neuromuscular junction (NMJ) integrity was assessed as a ratio of the number of innervated NMJs (seen by full colocalization of presynaptic axonal and postsynaptic acetylcholine receptor markers) (Fig. S6*A*) divided by the total number of postsynaptic receptor sites per field (Fig. S6*B*) in αS intramuscular (IM)-injected $M83^{+/-}$ Tg mice ($n = 10$) and age-matched, naive $M83^{+/-}$ Tg mice ($n = 10$).

Motor Neuron Counting. The entire lumbar region of each mouse spinal cord was paraffin-embedded and consecutive-sectioned (7 μm). These sections were deparaffinized and hydrated through a series of graded ethanol solutions. The sections were incubated in 0.1% Luxol fast blue solution at 56 °C overnight. After rinsing in distilled water, sections are differentiated in 0.05% lithium carbonate and 70% (vol/vol) ethanol. Sections were counterstained with cresyl violet solution for 6 min before differentiation in 95% (vol/vol) ethanol and dehydration. The number of motor neurons from every tenth section of the lumbar cord was then counted from phenotypic IM-injected M83 Tg mice ($n = 6$) and from native nontransgenic (nTg) mice ($n = 4$). The data were then expressed as a ratio of the average number of motor neurons in the lumbar spine of M83 Tg mice to nTg mice. This comparison was used because it has been previously shown that aged, symptomatic (paralyzed) M83 Tg mice show no loss of motor neuron counts compared with nTg mice (10).

Double-Labeling Immunofluorescence Analysis of Mouse Brain Tissue. Paraffin-embedded tissue sections were deparaffinized and hydrated through a series of graded ethanol solutions followed by 0.1 M Tris (pH 7.6). The sections were blocked with 5% dry milk/0.1 M Tris (pH 7.6) and were incubated simultaneously with combinations of primary antibodies diluted in 5% dry milk/0.1 M Tris (pH 7.6). After extensive washing, sections were incubated with secondary antibodies conjugated to Alexa 594 or Alexa 488 (Invitrogen). Sections were postfixed with formalin, incubated with Sudan Black, and stained with 5 μg/mL 4′,6-diamindino-2-phenylindole (DAPI). The sections were cover-slipped with Fluoromount-G (SouthernBiotech) and visualized using an Olympus BX51 microscope mounted with a DP71 Olympus digital camera to capture images.

Antibodies. pSer129/81A is a mouse monoclonal antibody that recognized αS phosphorylated at Ser129 (12). SNL-4 is a rabbit polyclonal antibody raised against a synthetic peptide corresponding to amino acids 2–12 of αS (6). Syn506 is an anti–N-terminal αS antibody that preferentially detects αS in pathological inclusions (7). Anti-p62 (SQSTM1; Proteintech), anti-glial fibrillary acidic protein (GFAP) (Promega), and anti-ionized calcium-binding adaptor molecule 1 (Iba-1) (DAKO) are rabbit polyclonal antibodies. Anti-choline acetyltransferase (CHAT) (Millipore) is a goat polyclonal antibody. Chicken polyclonal anti-neurofilament-H antibody was obtained from Encore Biotechnology and a mouse monoclonal anti-syntaptotagmin antibody was from the Developmental Studies Hybridoma Bank.

1. Giasson BI, Murray IV, Trojanowski JQ, Lee VMY (2001) A hydrophobic stretch of 12 amino acid residues in the middle of alpha-synuclein is essential for filament assembly. *J Biol Chem* 276(4):2380–2386.
2. Waxman EA, Mazzulli JR, Giasson BI (2009) Characterization of hydrophobic residue requirements for alpha-synuclein fibrillization. *Biochemistry* 48(40):9427–9436.
3. Greenbaum EA, et al. (2005) The E46K mutation in alpha-synuclein increases amyloid fibril formation. *J Biol Chem* 280(9):7800–7807.
4. Luk KC, et al. (2009) Exogenous alpha-synuclein fibrils seed the formation of Lewy body-like intracellular inclusions in cultured cells. *Proc Natl Acad Sci USA* 106(47): 20051–20056.
5. Waxman EA, Giasson BI (2010) A novel, high-efficiency cellular model of fibrillar alpha-synuclein inclusions and the examination of mutations that inhibit amyloid formation. *J Neurochem* 113(2):374–388.
6. Giasson BI, et al. (2000) A panel of epitope-specific antibodies detects protein domains distributed throughout human alpha-synuclein in Lewy bodies of Parkinson's disease. *J Neurosci Res* 59(4):528–533.
7. Waxman EA, Duda JE, Giasson BI (2008) Characterization of antibodies that selectively detect alpha-synuclein in pathological inclusions. *Acta Neuropathol* 116(1):37–46.
8. Sacino AN, et al. (2013) Conformational templating of α-synuclein aggregates in neuronal-glial cultures. *Mol Neurodegener* 8:17.
9. Crystal AS, et al. (2003) A comparison of amyloid fibrillogenesis using the novel fluorescent compound K114. *J Neurochem* 86(6):1359–1368.
10. Giasson BI, et al. (2002) Neuronal alpha-synucleinopathy with severe movement disorder in mice expressing A53T human alpha-synuclein. *Neuron* 34(4):521–533.
11. Valdez G, et al. (2010) Attenuation of age-related changes in mouse neuromuscular synapses by caloric restriction and exercise. *Proc Natl Acad Sci USA* 107(33):14863–14868.
12. Waxman EA, Giasson BI (2008) Specificity and regulation of casein kinase-mediated phosphorylation of alpha-synuclein. *J Neuropathol Exp Neurol* 67(5):402–416.

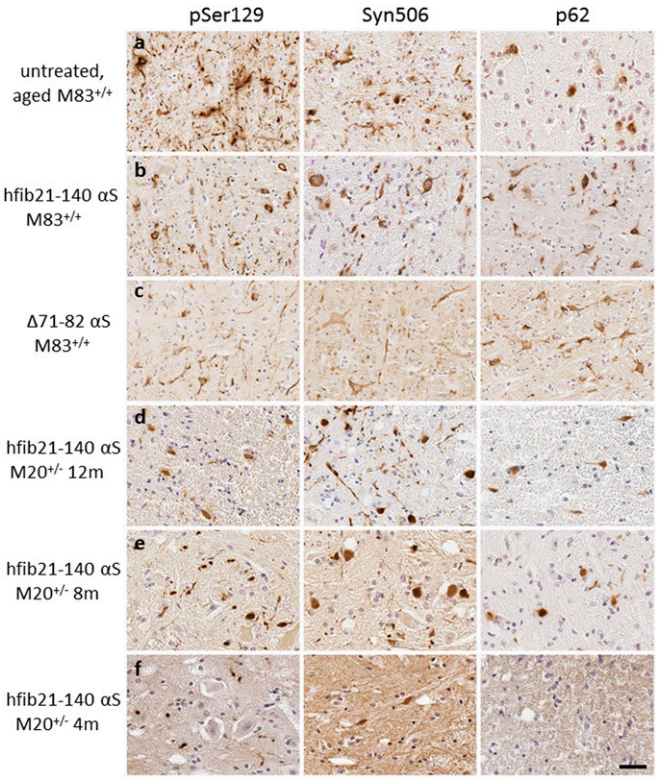

Fig. S1. αS pathology in injected M83$^{+/+}$ and M20$^{+/-}$ Tg mice is detectable with multiple markers for mature αS pathology. Representative images of brainstem tissue sections from a 15-mo-old, untreated M83$^{+/+}$ Tg mouse that developed motor impairments (*A*), an M83$^{+/+}$ Tg mouse that is 2 mo post-IM (biceps femoris muscle) injection with hfib21-140 αS (*B*), and an M83$^{+/+}$ Tg mouse that is 4 mo postinjection (biceps femoris muscle) with Δ71–82 αS (*C*); and cervical spinal cord tissue sections from M20$^{+/-}$ Tg mice that are 12 mo (*D*), 8 mo (*E*), and 4 mo (*F*) postinjection (biceps femoris muscle) hfib21-140 αS. Sections were stained with three separate markers for mature αS pathology: pSer129/81A, an antibody detecting αS inclusions that are hyperphosphorylated at Ser129 (1, 2); Syn506, an antibody that specially recognized the N terminus of αS (3); and p62, an antibody that nonspecifically recognizes intracellular protein aggregates (4). Each marker was able to detect αS pathology with similar staining densities in untreated and injected M83 Tg$^{+/+}$ mice, and 8 mo- and 12 mo-injected M20 Tg mice. In M20$^{+/-}$ Tg mice 4 mo after injection, inclusions were not stained with p62 antibodies. (Scale bar: 50 μm.)

1. Waxman EA, Giasson BI (2010) A novel, high-efficiency cellular model of fibrillar alpha-synuclein inclusions and the examination of mutations that inhibit amyloid formation. *J Neurochem* 113(2):374–388.
2. Waxman EA, Giasson BI (2008) Specificity and regulation of casein kinase-mediated phosphorylation of alpha-synuclein. *J Neuropathol Exp Neurol* 67(5):402–416.
3. Waxman EA, Duda JE, Giasson BI (2008) Characterization of antibodies that selectively detect alpha-synuclein in pathological inclusions. *Acta Neuropathol* 116(1):37–46.
4. Kuusisto E, Parkkinen L, Alafuzoff I (2003) Morphogenesis of Lewy bodies: dissimilar incorporation of alpha-synuclein, ubiquitin, and p62. *J Neuropathol Exp Neurol* 62(12):1241–1253.

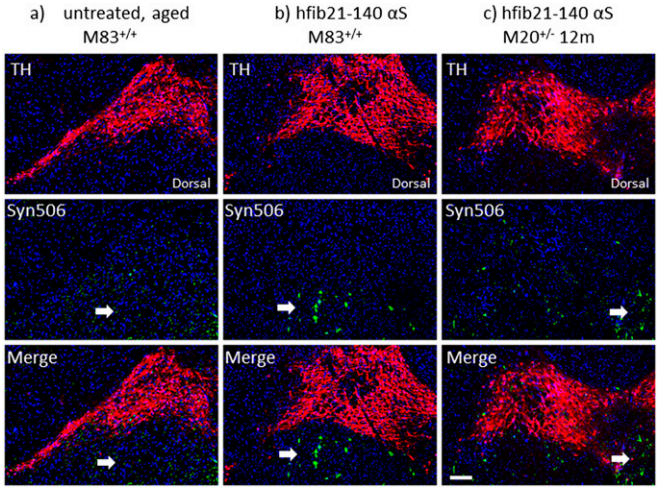

Fig. S2. αS inclusions in the substantia nigra region of $M83^{+/+}$ and $M20^{+/-}$ Tg mice are not found in dopaminergic neurons. Midbrain tissue sections from a 15-mo-old untreated, aged M83 $Tg^{+/+}$ mouse that developed motor impairments (*A*) and an $M83^{+/+}$ Tg mouse that is 2 mo postinjection (*B*) and an $M20^{+/-}$ Tg mouse that is 12 mo postinjection (*C*) with hfib21-140 αS. Double immunofluorescent labeling of dopaminergic neurons of the substantia nigra with tyrosine hydroxylase (TH; red) and Syn506 (green) shows that αS inclusions are predominantly found dorsal to the substantia nigra in the midbrain (arrows indicate the dorsal aspect of the midbrain region). Overlay images are shown in the bottom panels. (Scale bar: 100 μm.)

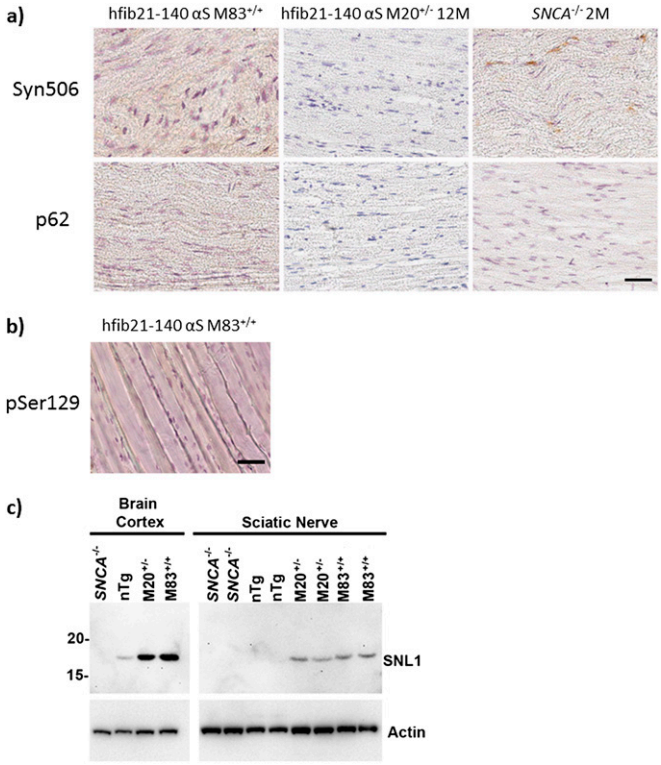

Fig. S3. αS inclusions are not present in the sciatic nerve or skeletal muscle of M83 or M20 Tg mice following IM injection of fibrillar αS. (*A*) Motor-impaired hfib21-140 αS-injected M83$^{+/+}$ and M20$^{+/-}$ Tg mice with robust CNS αS pathology did not exhibit any pathology in the sciatic nerve at the time of demise and revealed similar staining as untreated *SNCA*$^{-/-}$ controls. Similarly, no αS pathology could be detected in the sciatic nerve of M83$^{+/-}$ Tg mice injected with αS fibrils. pSer129 staining was not used to detect αS inclusion pathology in sciatic nerve due to cross-reactive staining with phosphorylated low molecular mass neurofilament subunit, which is abundant in white matter tracts (1). (*B*) No αS inclusion pathology was observed in the skeletal hind limb muscles of M83$^{+/+}$ Tg mice postinjection of hfib21-140 αS at the time when the mice were harvested. Similarly, no αS inclusion pathology was detected with antibody Syn 506 or in any M83$^{+/-}$ or M20$^{+/-}$ Tg IM-injected with fibrillar αS. (*C*) In both M83$^{+/+}$ and M20$^{+/-}$ Tg mice, αS expression is found in the sciatic nerve; however, expression is lower than in brain and it was not detected in nTg mice. Equal amounts (7.5 μg) of total SDS-soluble total protein extracts from the brain cortex or sciatic nerve of individual M20$^{+/-}$ and M83$^{+/+}$ Tg, nTg, and αS-null mice (SNCA$^{-/-}$) (2) were loaded on separate lanes of an SDS-polyacrylamide gel and analyzed by immunoblotting with antibody SNL1 that detects both murine and human αS (3) or an antibody (clone C4) (Millipore) to total actin as a loading control. The motilities of molecular mass markers are indicated on the left. (Scale bars: 100 μm.)

1. Sacino AN, et al. (2014) Amyloidogenic α-synuclein seeds do not invariably induce rapid, widespread pathology in mice. *Acta Neuropathol* 127(5):645–665.
2. Abeliovich A, et al. (2000) Mice lacking alpha-synuclein display functional deficits in the nigrostriatal dopamine system. *Neuron* 25(1):239–252.
3. Giasson BI, et al. (2000) A panel of epitope-specific antibodies detects protein domains distributed throughout human alpha-synuclein in Lewy bodies of Parkinson's disease. *J Neurosci Res* 59(4):528–533.

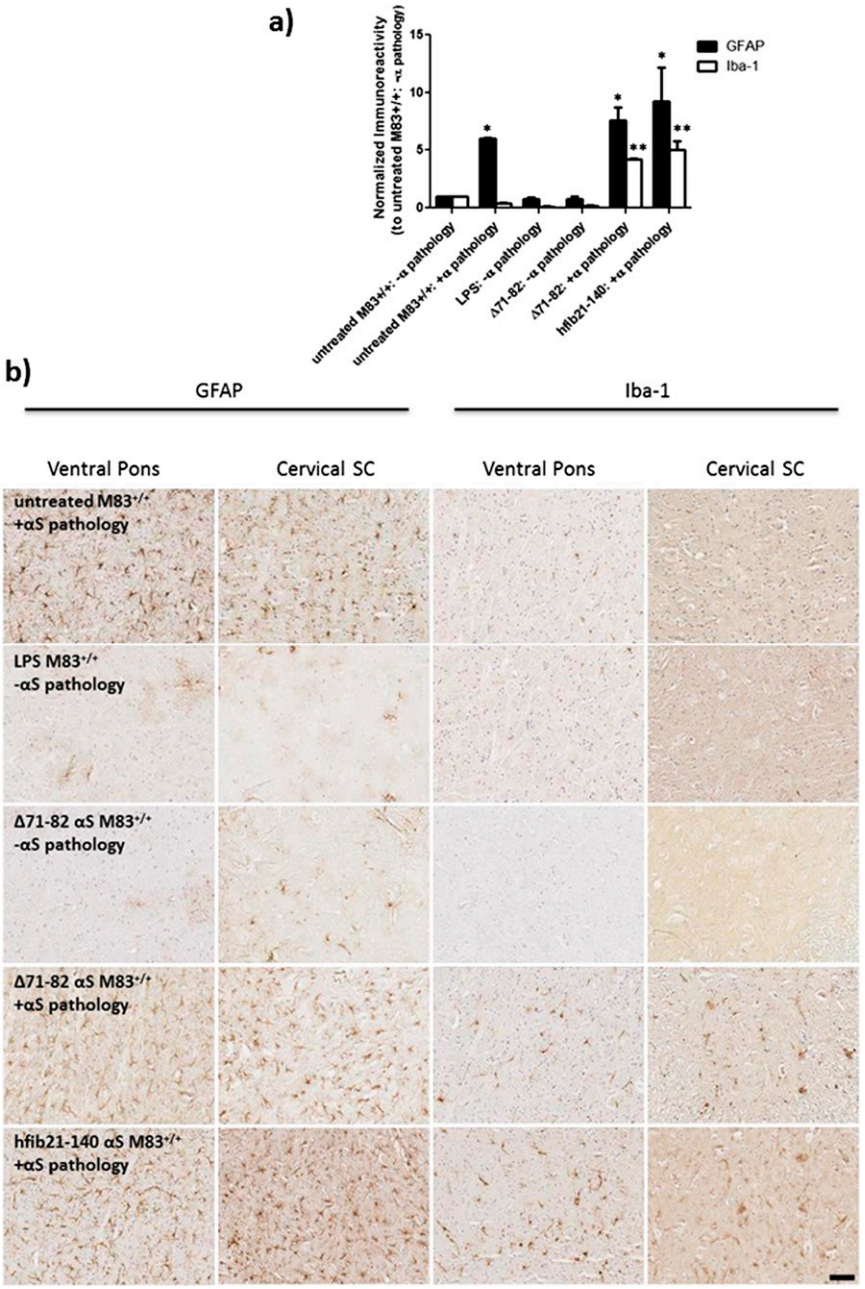

Fig. S4. Accelerated onset of astrogliosis and induction of microgliosis in M83$^{+/+}$ Tg mice IM-injected with Δ71–82 αS and hfib21-140 αS compared with untreated, aged M83$^{+/+}$ Tg mice. (*A*) For each condition, quantitative analyses of GFAP immunoreactivity, a marker of the astrogliosis, and Iba-1 immunoreactivity, a marker of microgliosis, per area were performed and normalized relative to the staining signal in untreated M83$^{+/+}$ Tg mice without αS inclusion pathology. M83$^{+/+}$ Tg mice IM-injected with either Δ71–82 αS or hfib21-140 αS and that develop robust αS CNS inclusion pathology demonstrated a six- to eightfold increase in the abundance of GFAP staining signal similar to that seen in untreated, aged M83$^{+/+}$ Tg mice that presented with αS inclusion pathology (associated with aging and motor impairment) (*$P < 0.001$). Mice IM-injected with αS protein and that developed CNS αS inclusion pathology also showed an approximately fivefold increase in Iba-1 staining signal, which was not seen in motor impairment untreated, aged M83$^{+/+}$ Tg mice (**$P < 0.001$). No quantitative increase in GFAP or Iba-1 staining was observed in M83$^{+/+}$ Tg mice IM-injected with LPS or Δ71–82 αS and that did not develop CNS αS inclusion pathology. (*B*) Representative images of ventral pons or cervical spinal cord tissue sections stained by immunohistochemistry (IHC) for GFAP or Iba-1. In untreated, aged M83$^{+/+}$ Tg mice with robust αS pathology in the pons and spinal cord, there is increased astrogliosis in the pons and gray matter of the spinal cord with limited microgliosis. M83$^{+/+}$ Tg mice IM-injected with 10 μg of LPS or 10 μg of Δ71–82 αS that has no αS inclusion pathology at 4 mo postinjection showed baseline levels of astrocytes and microglia in the pons and spinal cord. M83$^{+/+}$ Tg mice IM-injected with 10 μg of Δ71–82 αS or 10 μg of hfib21-140 αS that developed αS pathology demonstrated elevated astrogliosis and increased microgliosis in both these affected areas. (Scale bar: 100 μm.)

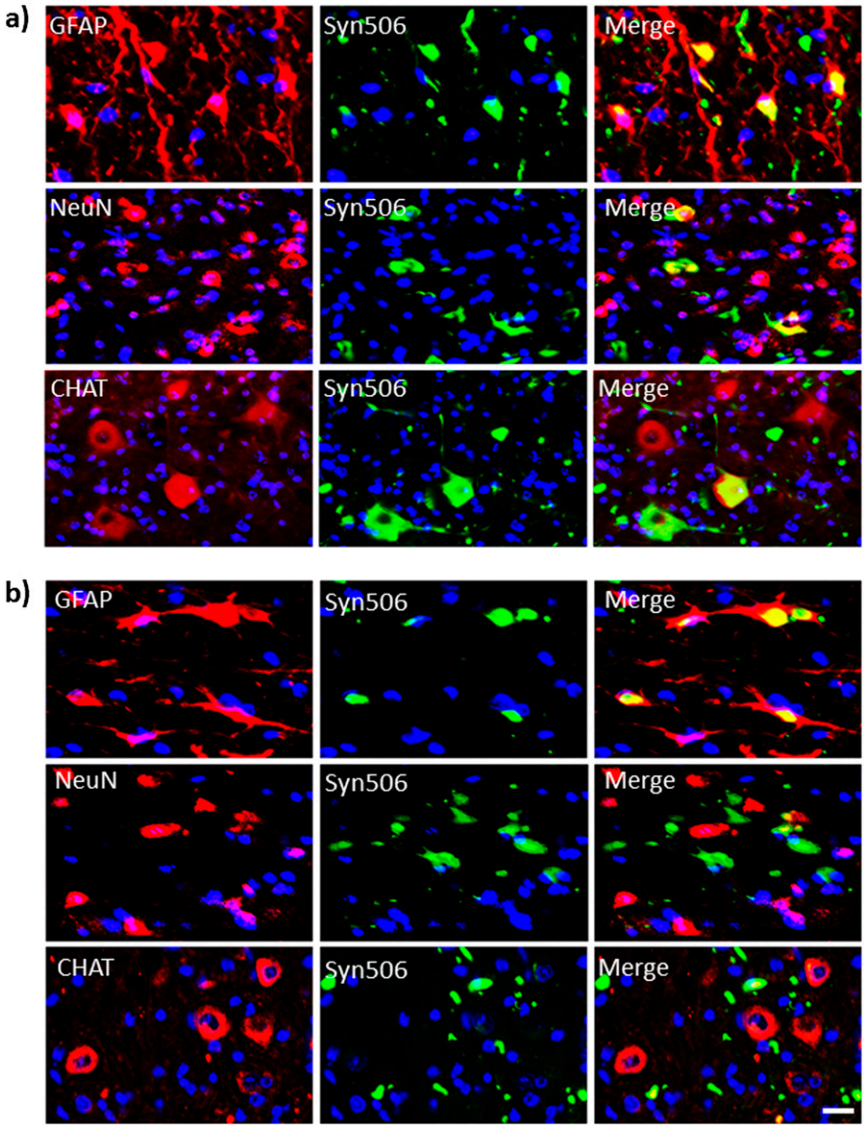

Fig. S5. αS inclusion pathology is found in multiple cell types postinjection of fib αS in both $M83^{+/+}$ and $M20^{+/-}$ Tg mice. Double immunofluorescence analysis of cervical spinal cord tissue from an $M83^{+/+}$ Tg mouse that is 2 mo postinjection (*A*) and an $M20^{+/-}$ Tg mouse that is 12 mo postinjection (*B*) of 10 μg of hfib21-140 αS. In $M83^{+/+}$ Tg mice, Syn506+ αS inclusions were found in both astrocytes (GFAP) and neurons (NeuN), particularly in motor neurons in the ventral horn of the spinal cord (CHAT). In $M20^{+/-}$ Tg mice, Syn506+ αS inclusions were frequently found in astrocytes and to a lesser extent in neurons; however, rarely were any αS inclusions found in motor neurons. Tissue sections were counterstained with DAPI (blue). (Scale bar: 50 μm.)

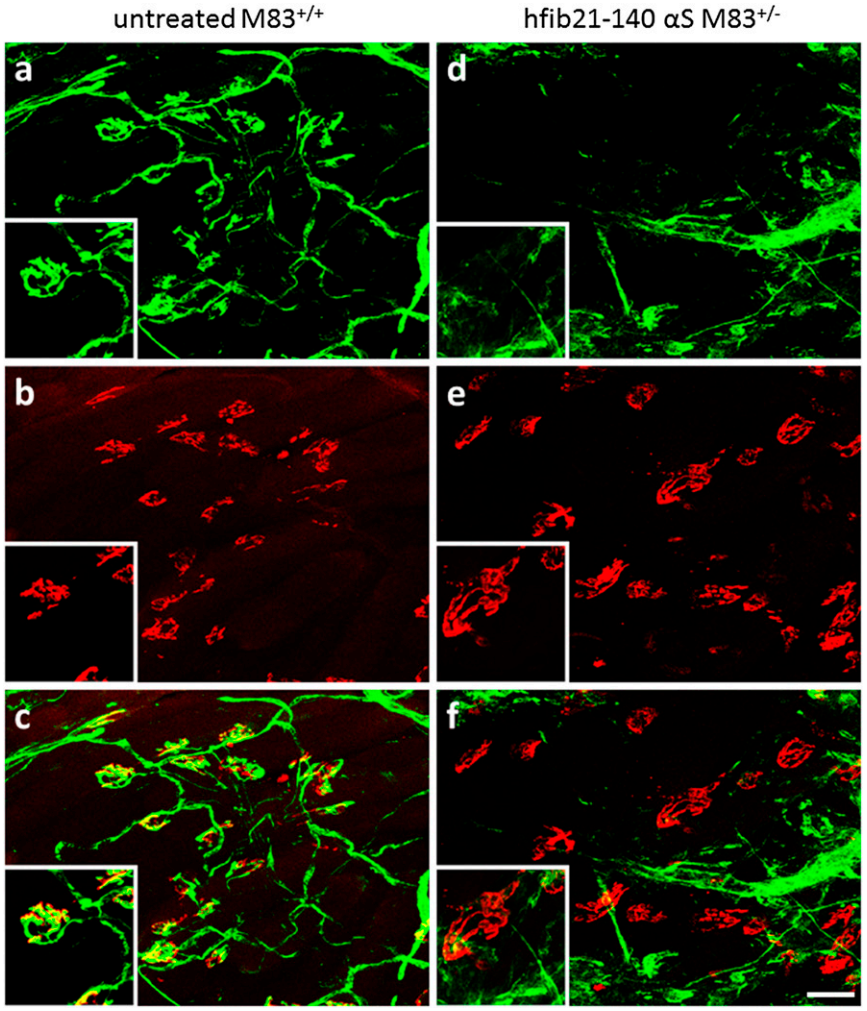

Fig. S6. Loss of intact NMJ in M83$^{+/-}$ Tg mice after injection of 10 μg of hfib21-140 αS. Double-immunofluorescence analysis of the digitorum brevis muscles of untreated M83$^{+/+}$ Tg mice and injected M83$^{+/-}$ Tg mice was used to detect the presynaptic motor neuron axon (neurofilament H and syntaptotagmin; green; *A* and *D*) and the postsynaptic acetylcholine receptor (α-bungarotoxin; red; *B* and *E*) of the NMJ. In the native M83$^{+/+}$ Tg mice, the NMJs were fully innervated as shown by colocalization of motor neuron axonal markers with postsynaptic receptors (*C*). However, in the M83$^{+/-}$ Tg mice IM injected with hfib21-140 αS and exhibiting a progressive, degenerative motor phenotype, there was dramatic withdrawal of motor neuron axons from the postsynaptic sites (*F*). (Scale bar: *A–F*, 50 μm; *Insets*, 25 μm.)

Table S1. Summary of M83 Tg mice injected with αS proteins and LPS control

Strain	Inoculum	Muscle site of injection	No. of mice	Median survival, dpi	Phenotype	Pathology
M83$^{+/+}$ (A53T αS)	Bilateral hfib21-140-αS (5 μL of 2 mg/mL)	Biceps femoris	15	77	12 of 15 with foot drop/paralysis*	12 of 15 with robust αS pathology*
M83$^{+/+}$ (A53T αS)	Bilateral mfib-αS (5 μL of 2 mg/mL)	Biceps femoris	7	53	7 of 7 with foot drop/paralysis	7 of 7 with robust αS pathology
M83$^{+/+}$ (A53T αS)	Unilateral mfib-αS (5 μL of 2 mg/mL)	Gastrocnemius	9	56	8 of 9 with foot drop/paralysis[†]	8 of 9 with robust αS pathology[†]
M83$^{+/+}$ (A53T αS)	Bilateral Δ71–82 αS (5 μL of 2 mg/mL)	Biceps femoris	11	120	2 of 11 with foot drop/paralysis[‡]	5 of 11 with αS pathology[§]
M83$^{+/+}$ (A53T αS)	Bilateral LPS (5 μL of 5 mg/mL)	Biceps femoris	5	Harvested at 123 dpi	0 of 5 with foot drop/paralysis	0 of 5 with αS pathology
M83$^{+/-}$ (A53T αS)	Bilateral hfib21-140-αS (5 μL of 2 mg/mL)	Gastrocnemius	10	111	10 of 10 with foot drop/paralysis	10 of 10 with robust αS pathology
M83$^{+/-}$ (A53T αS)	Unilateral mfib-αS (5 μL of 2 mg/mL)	Gastrocnemius	10	129	10 of 10 with foot drop/paralysis	10 of 10 with robust αS pathology
M83$^{+/-}$ (A53T αS)	Unilateral mfib-αS (5 μL of 2 mg/mL) SNT[¶]	Gastrocnemius	7	Undefined[‖]	3 of 7 mice with foot drop/paralysis**	3 of 7 mice with robust αS pathology**

M83 Tg mice received injections at 2 mo of age. See Fig. 2 for pathology distribution.
*Two mice died suddenly without an observed phenotype and were not available to analyze for αS pathology.
[†]One mouse died suddenly without an observed phenotype and was not available to analyze for αS pathology.
[‡]Two of these mice had a similar foot drop phenotype and extensive hind limb paralysis as mice injected with fib αS, and an additional four mice were moribund with more subtle muscle weakness, but without obvious foot drop or paralysis. They were killed upon veterinary recommendation.
[§]Two of these mice had widespread αS pathology as described in Fig. 2*C*. Three additional mice without a phenotype had αS pathology in the same area, but less abundant.
[¶]SNT, sciatic nerve transection.
[‖]Four mice in the cohort are still living with no sign of any degenerative phenotype.
**See Fig. 3.

Table S2. Summary of M20 Tg mice injected with αS proteins and PBS control

Strain	Inoculum	Muscle site of injection	No. of mice	Harvest time point, dpi	Phenotype	Pathology
M20$^{+/-}$ (WT αS)	Bilateral PBS (5 μL)	Biceps femoris	5	360	0 of 5 with foot drop/paralysis	0 of 5 with αS pathology
M20$^{+/-}$ (WT αS)	Bilateral Δ71–82 αS (5 μL of 2 mg/mL)	Biceps femoris	5	360	0 of 5 with foot drop/paralysis	1 of 5 with rare αS inclusions in spinal cord*
M20$^{+/-}$ (WT αS)	Bilateral hfib21-140-αS (5 μL of 2 mg/mL)	Biceps femoris	7	120	0 of 7 with foot drop/paralysis	1 of 7 with sparse αS inclusions in spinal cord*
M20$^{+/-}$(WT αS)	Bilateral hfib21-140-αS (5 μL of 2 mg/mL)	Biceps femoris	5	240	0 of 5 with foot drop/paralysis	5 of 5 with moderate spinal cord and brain αS pathology
M20$^{+/-}$(WT αS)	Bilateral hfib21-140-αS (5 μL of 2 mg/mL)	Biceps femoris	5	360	0 of 5 with foot drop/paralysis	5 of 5 with moderate spinal cord and brain αS pathology

M20 Tg mice received injections at 2 mo of age. See Fig. 4 for pathology distribution.
*These inclusions in spinal cord were detected with αS antibodies but not antibodies to the general inclusion marker p62 (Fig. 4 and Fig. S1).

Table S3. Summary of IM-injected nTg and *SNCA*$^{-/-}$ mice

Strain	Inoculum	Muscle site of injection	No. of mice	Harvest time point, dpi	Phenotype	Pathology
nTg	Bilateral hfib-αS (5 μL of 2 mg/mL)	Biceps femoris	5	360	0 of 5 with foot drop/paralysis	0 of 5 with αS pathology
nTg	Bilateral mfib-αS (5 μL of 2 mg/mL)	Biceps femoris	5	360	0 of 5 with foot drop/paralysis	0 of 5 with αS pathology
SNCA$^{-/-}$	Bilateral hfib-αS (5 μL of 2 mg/mL)	Biceps femoris	7	360	0 of 5 with foot drop/paralysis	0 of 5 with αS pathology

nTg and *SNCA*$^{-/-}$ mice received injections at 2 mo of age.

Movie S1. Bilateral hind limb foot drop and hind leg weakness in an M83$^{+/+}$ Tg mouse at 2 mo post IM injection of hfib21-140 αS. The foot drop progressed to paralysis and a moribund state within a week.

Movie S1